Chemical Engineering Journal 188 (2012) 15–22

Contents lists available at SciVerse ScienceDirect

Chemical Engineering Journal

journal homepage: www.elsevier.com/locate/cej

Removal of arsenite from aqueous solution by a zirconia nanoparticle

Yu-Ming Zheng, Ling Yu, Dan Wu, J. Paul Chen *

Department of Civil & Environmental Engineering, National University of Singapore, 10 Kent Ridge Crescent, Singapore 119260, Singapore

ARTICLE INFO

Article history:
Received 31 August 2011
Received in revised form
13 December 2011
Accepted 13 December 2011

Keywords:
Adsorption
Arsenite
Kinetics
Mechanism
Isotherm
Nanoparticle

ABSTRACT

This study evaluated the effectiveness of a readily prepared zirconia nanoparticle in removing arsenite (As(III)) from aqueous solution. It was demonstrated, without pre-oxidation of arsenite, the sorbent was highly effective for As(III) removal with a maximum adsorption capacity of 1.85 mmol-As/g. The sorbent had a high adsorption capacity toward As(III) at pH 5–10, and the optimal pH was around 8. The kinetics studies showed that most of the arsenite uptake occurred rapidly in the first 10 h, and the adsorption equilibrium was obtained within 48 h. The pseudo-second order model described the kinetics data well, and intraparticle diffusion model implied that two rate-limiting steps were involved in the sorption process. The adsorption isotherm data were well described by the Langmuir model. The adsorption was independent on ionic strength, implying As(III) may form inner-sphere complexes on the sorbent. The presence of humic acid or typical anions (e.g., fluoride, silicate, phosphate, and sulfate) did not greatly pose negative effects on the As(III) adsorption. However, the uptake of As(III) was hindered by the existence of bicarbonate. FTIR and XPS spectroscopic analyses suggested that hydroxyl and sulfate groups were involved in the As(III) uptake. Finally, an adsorption mechanism was proposed for better understanding on the adsorption of As(III).

1. Introduction

The arsenic contamination in water and its toxicity to human health have been well documented [1,2]. Consumption of either arsenic contaminated water or agricultural products irrigated by arsenic polluted water can cause serious human health problems [3–5]. A maximum contaminant level of 10 μg/L arsenic in drinking water has been adopted by the European Commission and the United States [6]. The stricter standard has initiated a series of R&D activities in order to obtain cost-effective arsenic treatment technologies.

Arsenic is ubiquitous in the environment, and the most common arsenic species in the water are inorganic arsenate (As(V)) and arsenite (As(III)), with arsenate prevailing in oxic waters and arsenite predominating in anaerobic waters [7–9]. It has been reported that arsenite can account for up to 67–99% of total arsenic species in ground water, which is a major source of drinking water throughout the world [7,10]. Compared with arsenate, arsenite is more toxic, mobile and difficult to be removed from waters [4,7].

Conventional arsenic removal technologies include coagulation [11], electro-coagulation [4,12], membrane filtration [13], and adsorption [6,14,15], etc. Due to the fact that arsenite exists in an uncharged form of H_3AsO_3 at the typical pH of water, the removal of As(III) is more difficult than that of As(V). To achieve higher As(III) removal efficiency, treatment processes generally include a pre-oxidation of arsenite to arsenate. Many oxidation technologies, including the injection of oxygen and/or ozone [10], Fenton process [16], biological oxidation [17], photocatalytic oxidation [18], the addition of conventional oxidants [19], and electro-oxidation [20], have been widely studied for the oxidation of As(III). Specifically, Kim and Nriagu reported the oxidation of arsenite in groundwater using ozone and oxygen [10]. They found that the half-lives of As(III) in experimental solutions saturated with ozone, pure oxygen and air were about 4 min, 2–5 days and 4–9 days, respectively. It was observed by Hug and Leupin [16], in a time scale of hours, As(III) was not oxidized by O_2 or H_2O_2, however, As(III) could be completely oxidized in the presence of Fe(II) and H_2O_2. Photocatalytic oxidation of arsenite and simultaneous removal of the generated arsenate from aqueous solution were reported by Zhang and Itoh [18]. It was found that, under UV-light irradiation, arsenite was firstly oxidized to arsenate and then was removed by the adsorbent. Sorlini and Gialdini reported that potassium permanganate and hypochlorite performed well for the oxidation of arsenite [19].

However, each of the abovementioned technologies faces one or more of the following limitations: (a) addition of oxidants or catalysts is needed for the oxidation; (b) extra energy input is needed in the photocatalytic or electro-oxidation process; (c) separation of the added catalyst may be required; or (d) some oxidants may lead

* Corresponding author. Tel.: +65 6516 8092; fax: +65 6774 4202.
E-mail addresses: paulchen@nus.edu.sg, jchen.enve97@gtalumni.org (J. Paul Chen).

1385-8947/$ – see front matter © 2011 Elsevier B.V. All rights reserved.
doi:10.1016/j.cej.2011.12.054

to the formation of toxic disinfection byproducts. Furthermore, the oxidized As(V) may be reduced to As(III) that becomes more mobile under certain conditions [21].

Recent progress in nanotechnology has led to a growing interest in the application of nanoscale adsorbents for arsenite removal. Pena et al. evaluated the effectiveness of titanium dioxide nanocrystalline in removing of arsenate and arsenite [22]. Their results demonstrated that nanocrystalline titanium dioxide was an effective adsorbent for As(V) and As(III) removal. Nanoscale zero-valent iron was synthesized and tested for As(III) removing by Kanel et al. [23]. It was found that the nanoscale zero-valent iron could be a suitable adsorbent for in situ and ex situ arsenite removal from groundwater. A hydrous nanostructure bimetal iron(III)–titanium(IV) oxides was fabricated and assessed for As(III) and As(V) removal from aqueous solution by Gupta and Ghosh [24], which demonstrated higher adsorption capacity for As(III) than As(V). Iron-doped activated carbon micro and nanoparticles were synthesized and tested for the removal of arsenic from contaminated water [25]. It had demonstrated that the methodology for the preparation of the nanoparticle was simple and up-scalable, and the developed adsorbent was efficient for arsenite removal. Manganese associated nanoparticles agglomerate of iron oxide was prepared and investigated for the adsorption of As(III) by Gupta et al. [26]. The optimum pH observed was 3.0–7.0 for the As(III) removal. Prasad et al. reported that a nano-sized iron oxides obtained from a cold rolling mill was cost-effective for the arsenite removal [27].

There is an increasing interest in the study of zirconium based sorbents for removal of As(V) from water solution, and the studies demonstrated zirconium based sorbents were effective for the adsorption of As(V) [6,28–30]. However, less studies on the As(III) adsorption have been reported. The aims of this study were devoted to develop and evaluate a promising zirconia nanoparticle sorbent for effective removal of As(III) without pre-oxidation.

In this study, to evaluate the As(III) adsorption behaviors on the zirconia nanoparticle, adsorption kinetics, isotherm, effect of pH, influence of natural organic matter (NOM) and coexisting anion were systematically studied. Furthermore, Fourier transform infrared spectroscopy (FTIR) and X-ray photoelectron spectroscopy (XPS) analyses were used to better understanding the adsorption mechanism.

2. Material and methods

2.1. Material

All chemicals were of analytical grade, which were purchased from Sigma–Aldrich and used as received without further purification.

The zirconia nanoparticle was synthesized following the below procedure [31]. First, a measured amount of zirconium oxychloride was dissolved in ultrapure water. After that, an acid was added under stirring, and zirconia nanoparticles were formed. The stirring continued for 2 h, and then the particles were washed with ultrapure water. Finally, the particles were harvested and dried for the subsequent experiments. Our previous study demonstrated that the size of zirconia nanoparticle was mainly between 60 and 90 nm.

2.2. Adsorption experiments

In the pH and ionic strength effect experiments, the arsenite solutions with different pH and background ionic strengths were prepared in glass bottles. HNO_3 or NaOH was used to adjust the pH of the solutions. Sodium perchlorate of 0, 0.005, or 0.05 M was used as ionic strength background. The sorbent was added into the As(III) solution, and then the mixtures were shaken at room temperature

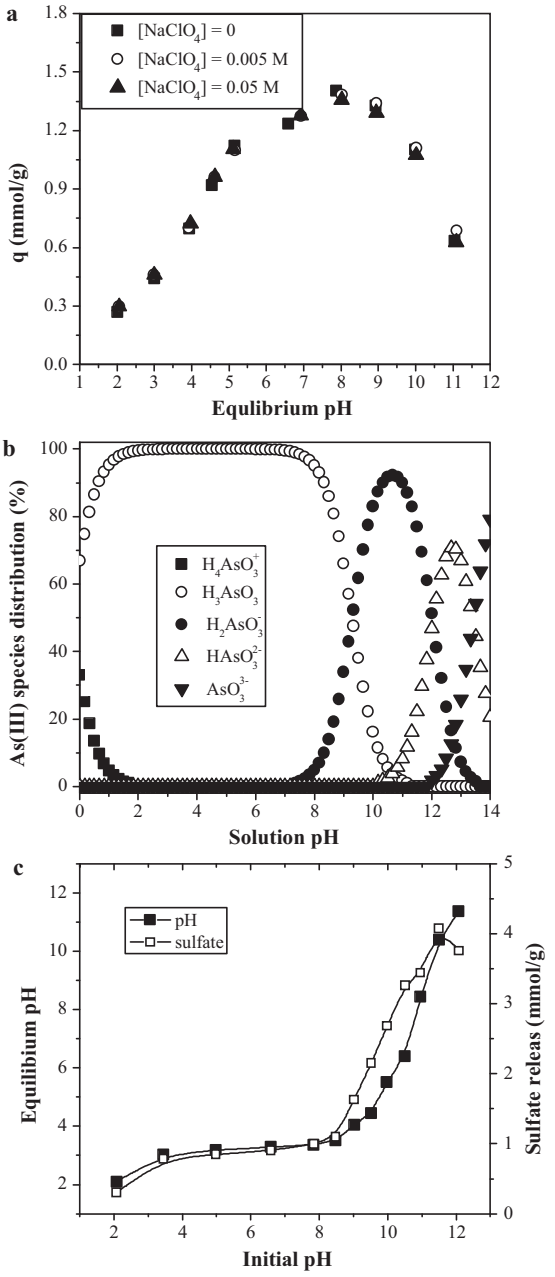

Fig. 1. Effect of pH and ionic strength on As(III) uptake: (a) experimental observation for arsenic uptake (pH was controlled); (b) As(III) species distribution as a function of pH by MINEQL; (c) change in pH and release of sulfate during As(III) uptake as a function of initial pH (pH was not controlled). Experimental conditions: sorbent dosage = 0.5 g/L, initial As(III) concentration = 1.0 mmol/L, $T = 25 \pm 1\,^{\circ}C$.

($T = 25 \pm 1\,^{\circ}C$) for 48 h. During the adsorption, the pH of the solution was maintained by adding HNO_3 or NaOH. At the end of the experiment, the samples were taken and filtered with 0.45 μm filter. The filtrate was then analyzed for residual arsenic and zirconium concentrations by inductively coupled plasma-optical emission spectrometer (ICP-OES, Thermo iCAP 6300). Furthermore, one more set of pH effect experiment was conducted, in which the solution pH was not maintained during the adsorption. The initial and equilibrium pHs of the solution were determined. The sulfur concentration at the end of the adsorption was also measured. The other procedure was the same as above.

In the kinetics experiment, 0.2 g sorbent was added into 1000 mL solution with an initial arsenite concentration of 0.5 mmol/L and pH of 8–9. The mixed solution was gently stirred. The samples were

collected at different time intervals, and analyzed for arsenic and sulfur concentrations by the ICP-OES. The equilibrium time for the adsorption was determined by the kinetics experiment.

In the adsorption isotherm experiment, 50 mL solutions with different arsenite concentration were prepared. The solution pH was adjusted to be 8–9. The sorbent with a mass of 0.025 g was added into each of the arsenite solution; the mixtures were shaken at room temperature for 48 h. Other procedures were the same as the pH effect experiments.

In the humic acid and coexisting anions effect experiments, 50 mL arsenite solutions with different concentration of humic acid or coexisting anion were prepared. The solution pH was adjusted to be 8–9. Twenty-five milligram of the sorbent was added into each of the arsenic solution; the mixtures were shaken at the room temperature for 48 h. Other procedures were the same as the pH effect experiments.

2.3. Spectroscopic analysis

Fourier transform infrared sand X-ray photoelectron spectroscopy were used to explore the interaction between As(III) and the sorbent. FTIR spectra of virgin and As-loaded sorbent were acquired with a Shimadzu FTIR spectrometer (IRPrestige-21) and a horizontal attenuated total reflectance (ATR) attachment (Pike) using a ZnSe reflection element. The background was automatically subtracted from the sample spectra. The spectra were collected within the wavenumber ranging from 650 to 4000 cm^{-1}. The spectra were recorded at a resolution of 4 cm^{-1} by co-adding 32 scans and plotted in the same scale on the transmittance axis. Moreover, the surfaces of virgin and As-loaded sorbent were analyzed using X-ray photoelectron spectroscopy (Kratos XPS system – Axis His-165 Ultra, Shimadzu), with a monochromatized Al Kα X-ray source (1486.6 eV). For wide scan XPS spectra, an energy range from 0 to 1100 eV was used with pass energy of 80 eV and step size of 1 eV. The high resolution scans were conducted according to the peak being examined with pass energy of 40 eV and step size of 0.05 eV. To compensate for charging effect, C 1s signal of an adventitious carbon was used as reference at a binding energy (BE) of 284.5 eV. The XPS results were collected in binding energy form and fit using a nonlinear least-square curve fitting program (XPSPEAK41 Software). For the element of oxygen, the spectra were deconvolved with the subtraction of a linear background. The peak's full-width-at-half-maximum (FWHM) was fixed during the fitting.

3. Results and discussion

3.1. Effect of pH and ionic strength

The distribution of arsenite species in solution and the surface properties of sorbent are generally highly pH-dependant. It is expected that the uptake of arsenite by the sorbent is associated with the solution pH. To evaluate the influence of pH on the arsenite uptake, several experiments were performed at different pH ranging from 2 to 11, and the obtained results are shown in Fig. 1a. It was found that the adsorption of As(III) by the sorbent was significantly affected by the solution pH. As the solution pH was raised from 2, the adsorption of arsenite increased. A maximum adsorption capacity was reached at an equilibrium solution pH of around 8. As the pH was further increased, the uptake of As(III) decreased. Similar trends have been found for arsenite adsorption onto an activated alumina grain by Lin and Wu [14].

The pH-dependent adsorption behavior may associate with the species distribution of arsenite and the surface properties of the sorbent. The sorbent has a point of zero charge pH (pH_{PZC}) of 2.85, which means the sorbent is positively charged as solution pH is lower than 2.85 and is negatively charged when solution pH is higher than 2.85 [31]. Hence, in most of the experimental pH range, the sorbent is negatively charged.

The acid–base dissociation constant (pK_a) values of arsenite are 9.22, 12.13 and 13.46, respectively [32]. Based on the pK_a values, the fractional distribution of As(III) species as a function of pH was calculated using MINEQL+ 4.5 [33], and the results were illustrated in Fig. 1b. The As(III) species can be in the forms of H_3AsO_3, $H_2AsO_3^-$, $HAsO_3^{2-}$, and AsO_3^{3-}, which is dependent on the solution pH. From pH 2 to 8, the neutral H_3AsO_3 is the dominant species in the aqueous solution. The electrostatic attraction between the negatively charged sorbent and the neutral As(III) species can be neglected. This indicates that the adsorption of As(III) onto the adsorbent is not due to the electrostatic interaction, and the uptake of As(III) onto the sorbent may be a chemisorption. According to Fig. 1b, the amount of negatively charged As(III) species is increased as the solution pH is higher than 8. There is a electrostatic repulsive between the electronegative As(III) species and the negatively charged sorbent. Therefore, the uptake of As(III) decreases as the solution pH is higher than 8.

In addition, another pH effect experiment was carried out, in which the solution pH was not maintained during the adsorption process. The initial pH versus final pH and the sulfate releasing as a function of initial pH are shown in Fig. 1c. It is demonstrated that the final pH is significantly lower than that of the initial pH, and the amount of sulfate released into the solution notably increases with an increasing solution pH. These results imply that hydrogen together with sulfate ions (in the form of bisulphate) are released into the solution during the adsorption process, which might be responsible for that the uptake of As(III) increases with an increasing pH from 2 to 8. The increasing pH facilitates the releasing of H^+ during the adsorption process.

In the pH effect experiments, the Zr concentration in the solution was measured after As(III) adsorption. It was observed that the level of Zr was below the detection limit of ICP-OES. This indicates that no zirconium is released from the sorbent in the experimental pH range.

Due to the existence of various ions in the natural waters, the background ionic strengths of the waters are different. It is important to evaluate the effect of background ionic strength on the adsorption of As(III) by the sorbent. On the other hand, ionic strength dependence studies on adsorption of adsorbates at the sorbent/aqueous interfaces can be a useful method for distinguishing between inner- and outer-sphere surface complexes [34].

According to the bonding affinity of ions for active sites on the sorbent surface, the adsorption can be classified into outer-sphere ion-pair complexes (weakly bonding) and inner-sphere surface coordination complexes (strongly bonding). In the inner-sphere complex adsorption, the strongly bonding anions are relatively unaffected or responded to higher ionic strength with greater adsorption. However, in the outer-sphere complex adsorption, the adsorption is suppressed by competition with background electrolyte and the adsorption can markedly be reduced by increasing the background ionic strength, since electrolyte may form outer-sphere complexes through electrostatic forces [5,34].

It is found in Fig. 1a that the increase in ionic strength from 0 to 0.05 M does not affect the adsorption of As(III) onto the sorbent. This suggests that the adsorption of As(III) onto the sorbent may be governed by inner-sphere complex adsorption mechanism.

3.2. Kinetics studies

The adsorption kinetics describes the rate of adsorbate uptake on the sorbent, which controls the adsorption equilibrium time. The kinetics parameters give important information for designing and modeling the adsorption process. The adsorption kinetics data

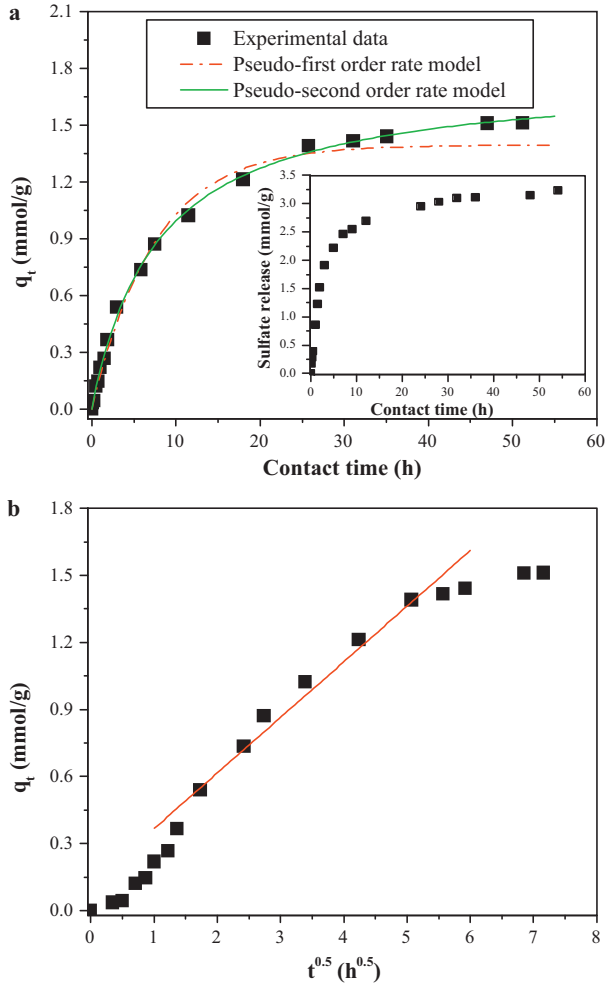

Fig. 2. Kinetics study of As(III) adsorption: (a) Experimental data and modeling result by pseudo-first order and pseudo-second order kinetics models (inset graph: release of sulfate); (b) Intraparticle diffusion plot. Experimental conditions: sorbent dosage = 0.2 g/L, initial As(III) concentration = 0.5 mmol-As/L, pH = 8–9, $T = 25 \pm 1$ °C.

were analyzed using different kinetics models including pseudo-first order model, pseudo-second order model and internal mass transfer model.

3.2.1. Pseudo-first order and pseudo-second order models

The expression of Lagergren pseudo-first order kinetics model is given by the following equation [35]:

$$q_t = q_e(1 - e^{-k_1 t}) \quad (1)$$

where k_1 (h^{-1}) is the first order rate constant, q_e (mmol/g) and q_t (mmol/g) are the amounts of adsorbate adsorbed at equilibrium and at any time, respectively. The value of q_e and k_1 can be obtained from the nonlinear curve fitting of experimental data q_t versus t.

The adsorption kinetics data were also analyzed by pseudo-second order model given by Ho and McKay [35] as follows:

$$q_t = \frac{k_2 q_e^2 t}{1 + q_e t} \quad (2)$$

where k_2 ((g/mmol)/h) is the rate constant of the pseudo-second order model. The nonlinear curve fitting of experimental data q_t against t can give the values of k_2 and q_e.

It can be found that most of the uptake of As(III) rapidly takes place in the first 10 h, followed by a relatively slow process. The adsorption can obtain pseudo steady state equilibrium within 48 h. The experimental data together with pseudo-first order and pseudo-second order model fitting curves are shown in Fig. 2a. The rate constants, calculated q_e and correlation coefficients obtained from the nonlinear curve fitting are summarized in Table 1. Fig. 2a shows that the pseudo-second order model fits the experimental data better than the pseudo-first order model. The pseudo-first order model fits the experimental data well in the initial rapid adsorption stage, and thereafter the fitting curve deviates from the experimental data. Whereas, the pseudo-second order model curve fits the experimental data well for the entire adsorption process. As shown in Table 1, the r^2 value for pseudo-second order model is higher than that of pseudo-first order model, demonstrating that the pseudo-second order model can be applied to describe the adsorption process. This indicates that the adsorption process might be chemisorptions.

In the adsorption kinetics study, the amount of sulfate released into the solution as a function of contact time was determined, and the results were illustrated in the inserted graph of Fig. 2a. It is found that the amount of sulfate released from the sorbent increases with an increasing contact time, suggesting the adsorption of As(III) leads to the releasing of sulfate from the sorbent. The amount of sulfate released is found to be around 3.0 mmol/g under adsorption equilibrium condition, which is around 2 times of the amount of As(III) adsorbed onto the sorbent.

3.2.2. Intraparticle diffusion model

The prediction of the rate-limiting step is important for designing an appropriate adsorption process. For a solid–liquid adsorption process, the adsorbate transfer is usually characterized by either external mass transfer (boundary layer diffusion), or intraparticle diffusion or both. The adsorption process can be divided into three consecutive steps as follows:

- Adsorbates are transported from bulk solution through liquid film to the adsorbent exterior surface (boundary layer diffusion), and instantaneous adsorption on the exterior surface.
- Diffusion of adsorbates into the pores of the sorbent (intraparticle diffusion).
- Uptake of adsorbates on the interior surface of the pores and capillary spaces of the sorbent.

The slowest step determines the rate-controlling parameter in the adsorption process. The intraparticle diffusion model proposed by Weber and Morris [36] is the most commonly used model to identify the mechanism involved in the sorption process. The intraparticle diffusion model can be expressed by Eq. (3).

$$q_t = k_{id} t^{1/2} + \alpha \quad (3)$$

where k_{id} ((mmol/g)/$h^{1/2}$)) is the intraparticle diffusion rate constant, α (mmol/g) is a constant in the intraparticle diffusion model which reflects the significance of boundary layer or external mass transfer effect.

Previous studies [37–40] demonstrated: (1) if the plot of q_t against $t^{0.5}$ gives a straight line, the adsorption process is only controlled by intraparticle diffusion; and (2) if the plot shows multi-linearity, two or more steps are involved in the sorption process. The plot of q_t of uptake of As(III) on the sorbent versus $t^{1/2}$ is illustrated in Fig. 2b. It was observed that the adsorption process tends to be divided into two phases: an initial smooth curve followed by a linear portion. The initial portion of the plot indicates the adsorption process is governed by boundary layer effect, whereas the second linear portion is controlled by intraparticle diffusion. The intraparticle diffusion rate constant k_{id} can be obtained from the slope of the linear portion. The intercept of the plot reflects the effect of the boundary layer. The larger the intercept, the greater

Table 1
Kinetics and isotherm model constants of As(III) uptake on the sorbent.

Kinetics	Pseudo-first order model	k_1 (1/h)	0.13
		$q_{e,cal}$ (mmol/g)	1.40
		r^2	0.993
	Pseudo-second order model	k_2 ((g/mmol)/h)	0.07
		$q_{e,cal}$ (mmol/g)	1.77
		r^2	0.998
	Intraparticle diffusion model	k_{id} ((mmol/g)/h$^{1/2}$)	0.249
		α (mmol/g)	0.118
		r^2	0.970
Isotherm	Langmuir	q_m (mmol/g)	1.85
		K_L (L/mmol)	30.1
		r^2	0.99
	Freundlich	K_F (mmol$^{(1-1/n)}$L$^{1/n}$/g)	2.00
		$1/n$	0.21
		r^2	0.98

the contribution of the boundary layer effect on the rate-limiting step. The values of k_{id} and α are summarized in Table 1.

3.3. Isotherm studies

The adsorption isotherm provides the most important piece of information in understanding an adsorption process. To understand the adsorption equilibrium, two most commonly used isotherm models, Langmuir and Freundlich, were employed to simulate the adsorption isotherms [41,42].

The linearized Langmuir and Freundlich isotherm are given by Eqs. (4) and (5), respectively.

$$\frac{c_e}{q_e} = \frac{1}{K_L q_m} + \frac{c_e}{q_m} \quad (4)$$

$$\lg\ q_e = \lg\ K_F + \frac{1}{n}(\lg\ c_e) \quad (5)$$

where c_e (mmol/L) is the equilibrium concentration of the adsorbate in solution, q_e (mmol/g) is the amount of the adsorbate adsorbed at the adsorbent, q_m (mmol/g) is the maximum amount of the adsorbate adsorbed at the adsorbent at equilibrium time, K_L (L/mmol) is a constant related to the heat of adsorption, K_F (mmol$^{(1-1/n)}$L$^{1/n}$/g) is related to the adsorption capacity of the adsorbent, and $1/n$ is a constant known as the heterogeneity factor that is related to the surface heterogeneity [39].

The calculated Langmuir and Freundlich isotherm constants and their corresponding linear regression correlation coefficient values are given in Table 1. Hence, the predicted Langmuir and Freundlich isotherm equations for As(III) adsorption onto the sorbent are given by Eqs. (6) and (7), which are useful for design of the adsorption process.

$$q_e = \frac{55.67 c_e}{1 + 30.09 c_e} \quad (6)$$

$$q_e = 2.00 c_e^{0.21} \quad (7)$$

The experimental data on adsorption isotherm together with the predicted Langmuir and Freundlich simulation curves are shown in Fig. 3. It was found that the maximum adsorption capacity of zirconia nanoparticle for As(III) was 1.85 mmol/g. A comparison of the maximum adsorption capacity for As(III) of the zirconia nanoparticle with some reported nanostructure adsorbents was summarized in Table 2. The q_m value shows that the maximum adsorption capacity of the sorbent is higher than most reported sorbents. The sorption equilibrium data fit Langmuir and Freundlich equations both well with a squared correlation coefficient value of 0.99 and 0.98, respectively. From Fig. 3, it is observed that the equilibrium data can be better described by Freundlich model at lower solute equilibrium concentrations, whereas the Langmuir model fit the equilibrium data better at higher concentrations.

Temperature may play an important role in the adsorption process. To investigate the effect of temperature on the As(III) adsorption by the sorbent, the isotherm studies were carried out at another three temperatures (35, 45 and 55 °C). The obtained results showed that the temperature did insignificant influence on the adsorption isotherm (figure not shown here), implying that the zirconia sorbent can be used for arsenite removal at a wide range of temperature.

3.4. Effect of natural organic matter and coexisting anions

Natural organic matters widely exist in the surface and ground waters. As the natural organic matters may have a high tendency to be adsorbed on the sorbent, which subsequently change the surface properties of the adsorbent and block the adsorption passages or active sites. Hence, in a natural aquatic environment, the adsorption behavior of adsorbate on sorbent may be greatly affected by the existence of NOM. Moreover, arsenite in contaminated ground water is usually accompanied with different anions (e.g. carbonate, fluoride, silicate, phosphate and sulfate), which may lead to compete with As(III) for the available active sites on the adsorbent. To obtain a better understanding on application of the sorbent for arsenite removal from natural aquatic environment, it is crucial to study the potential influences of NOM and coexisting anions on the arsenite adsorption.

The effect of NOM, represented by humic acid (HA), on the adsorption was investigated in this study. The obtained results demonstrate that the presence of 0–10 mg/L HA does not notably influence the adsorption of As(III) (figure not shown here),

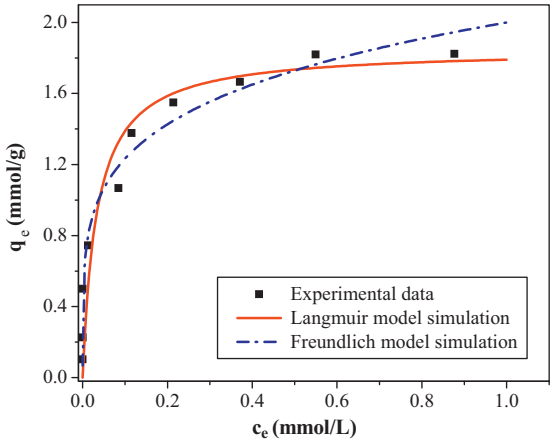

Fig. 3. Adsorption isotherm of As(III) on the sorbent. Experimental conditions: sorbent dosage = 0.5 g/L, pH = 8–9, and $T = 25 \pm 1$ °C.

Table 2
Comparison of maximum adsorption capacity for As(III) of zirconia nanoparticle with some reported nanostructure adsorbents.

Adsorbent	q_m (mmol/g)	pH	Ref.
Zirconia nanoparticle	1.85	8.0–9.0	Present work
Nanoscale zero-valent iron	0.024	7.0	[22]
Nanocrystalline titanium oxide	0.8	7.5	[23]
Nanostructure iron(III)–titanium(IV) oxide	1.13	7.0	[24]
Iron doped active carbon nanoparticle	0.20	7.0	[25]
Manganese associated hydrous iron(III) oxide	0.69	7.0 ± 0.1	[26]
Nano-sized Fe_2O_3	0.026	6.5	[27]

suggesting that the sorbent can be efficiently used for As(III) removal from natural waters containing NOM.

Typical anions, including bicarbonate, fluoride, silicate, phosphate and sulfate were selected as competition anions, their effects on the As(III) adsorption at pH 8–9 are investigated. The concentrations of the competition anions were prepared referred to their actual concentration levels in natural water environment. The presence of bicarbonate obvious decreases the uptake of As(III) onto the sorbent as shown in Fig. 4. The reduction of the amount of As(III) adsorbed may be due to that the competitive adsorption of bicarbonate onto the surface of sorbent. However, the adsorption of arsenite on the sorbent is not obviously influenced by the existence of fluoride (0–0.5 mmol/L), silicate (0–1.0 mmol/L), phosphate (0–0.5 mmol/L) and sulfate (0–1.0 mmol/L) (figure not shown here).

3.5. Spectroscopic analysis

FTIR and XPS analyses were employed to explore the interactions between As(III) and the sorbent, and the obtained results were shown in Figs. 5 and 6.

FTIR spectrum of virgin sorbent shown in Fig. 5 demonstrates a broad and strong absorption band in the range of 3000–3600 cm^{-1} (centered at 3300 cm^{-1}), which is responsible for the O–H stretching vibration, indicating the presence of hydroxyl group and small amount of water molecular on the surface of the sorbent. The peak at 1630 cm^{-1} could be assigned to the deformation vibration of water molecules (H–O–H bending), suggesting the physical adsorption of water on the zirconia sorbent, which is consistent with the band at 3400–3600 cm^{-1}. Peak at 1120 cm^{-1} can be assigned to SO_4^{2-}, which is in accordance with the chemical composition of the sorbent.

Compared with the FTIR spectrum of virgin sorbent, a small new band at the wavenumber of 816 cm^{-1} appears in the spectrum of

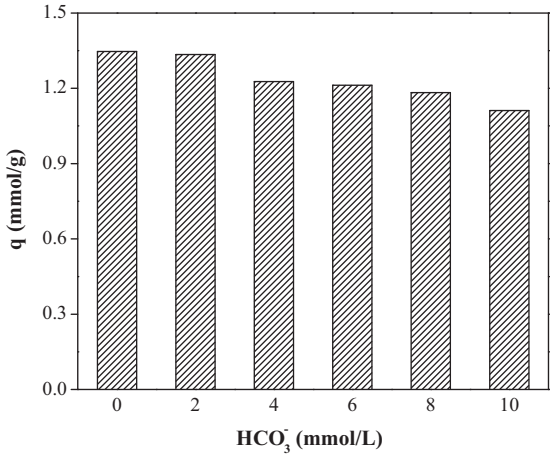

Fig. 4. Effect of bicarbonate on the adsorption of As(III). Experimental conditions: initial As(III) concentration = 1.1 mmol-As/L, solution pH = 8–9, and contact time = 2 days.

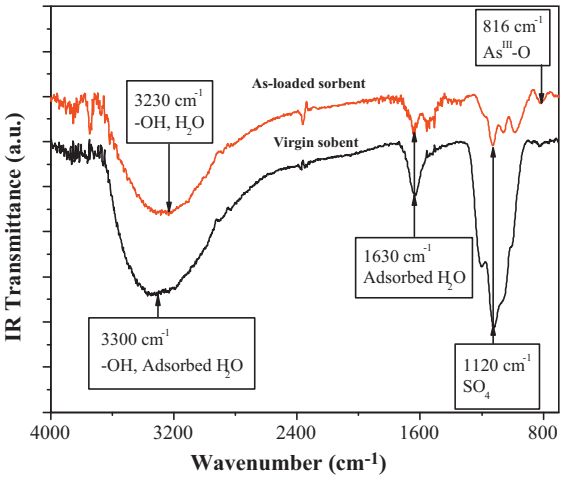

Fig. 5. FTIR spectra of virgin and As(III)-loaded sorbent.

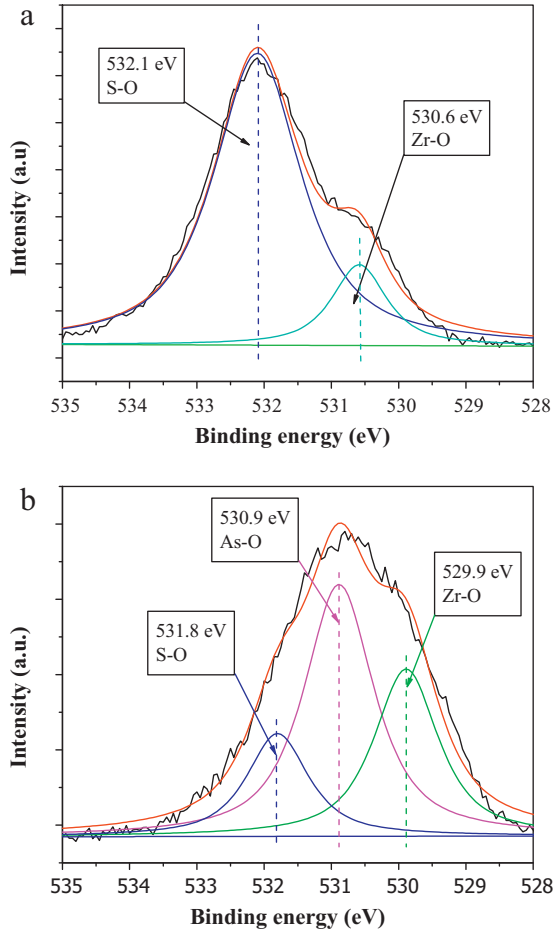

Fig. 6. O 1s core-level XPS spectrum of (a) virgin sorbent, (b) AS(III)-loaded sorbent.

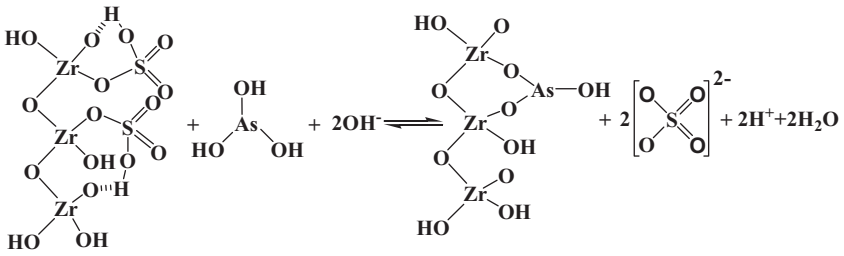

Fig. 7. Schematic diagram of adsorption mechanism of As(III) on the sorbent.

As(III)-loaded sorbent. It was reported that the absorption band assigned to the stretching vibration of As–O bond was located in the 750–950 cm^{-1} spectral range [43].

A broad absorption band near 816 cm^{-1} corresponding to asymmetrical stretch of As–OH was observed after the adsorption of As(III) onto surfactant-mediated akaganeite by Deliyanni et al. [44]. Hence, the new band can be assigned to the stretching vibration of As–O in arsenite, which demonstrates the loading of arsenite on the sorbent. The intensity of absorption band around 1120 cm^{-1} decreases significantly, indicating the obvious reduction of sulfate in the sorbent which resulted from the release of sulfate into the solution during the adsorption. The pH effect and kinetics study also demonstrated that the sulfate ions were released into the solution during the adsorption. These results indicate that an anion exchange mechanism is involved during the adsorption of As(III) onto the sorbent. The spectrum also illustrates the absorption band from 3400 to 3600 cm^{-1} becomes smaller and the center shifts from 3300 to 3230 cm^{-1}, indicating –OH on the surface of sorbent may be involved in the As(III) adsorption.

The wide scan XPS spectra showed that the main elements detected were O, S and Zr in the virgin sorbent, whereas the main elements detected in the As-loaded sorbent were O, S, Zr and As (figure not shown here). Compared with virgin sorbent, the amount of S decreased obviously. This results confirm the uptake of As(III) on the sorbent and the release of sulfate from the sorbent.

The O 1s core level XPS spectrum of the fresh sorbent can be decomposed into two component peaks as illustrated in Fig. 6a. The peaks with binding energy of 530.6 and 532.1 eV are assigned to the O 1s in the forms of Zr–O and O–S, respectively. Compared with the spectrum of virgin sorbent, the O 1s core level XPS spectrum of As(III)-loaded sorbent can be deconvolved into three components peaks with binding energy of 529.9, 530.9, and 531.8 eV, which are assigned to the oxygen in the form of S–O, As–O and Zr–O, respectively (Fig. 6b). This confirms the loading of As(III) onto the surface of the sorbent. It is also found that the intensity of oxygen peaks in the form of S–O reduces significantly after the adsorption, which results from the release of sulfate into the solution during the adsorption.

From the above experimental results and spectroscopic analysis, a concept of mechanism for the uptake of As(III) by the sorbent can be deduced (Fig. 7). The arsenite competes with sulfate for the active adsorption sites on the zirconia, and the adsorption of As(III) onto the sorbent leads to the release of HSO_4^- from the zirconia. The release of HSO_4^- results in a decrease in solution pH and an increase in the sulfate concentration. The adsorbed As(III) may form bidentate inner-sphere complexes on the surface of the sorbent.

4. Conclusions

The zirconium nanoparticle was demonstrated to be effective for As(III) removal without pre-oxidation. The As(III) adsorption was highly pH-dependent, and the optimal pH was around 8. The kinetics studies showed that most of the arsenite uptake rapidly occurred in the first 10 h, and the adsorption equilibrium was obtained within 48 h. The adsorption kinetics was well described by pseudo-second order model, and intraparticle diffusion model analysis implied that two rate-limiting steps were involved. The Langmuir model well described the isotherm data, and the maximum adsorption capacity was determined to be 1.85 mmol-As/g.

The increase of background ionic strength did not affect the adsorption, which implied that the adsorbed As(III) may form inner-sphere complexes on the sorbent. The presence of humic acid or typical anions (e.g. fluoride, silicate, phosphate, and sulfate) did not pose significantly negative effect on the adsorption. However, the existence of bicarbonate decreased the uptake of As(III).

FTIR and XPS spectroscopic analyses suggested that hydroxyl and sulfate groups were involved in the adsorption. Mechanisms for the uptake of As(III) was deduced. The arsenite competed with sulfate for the active adsorption sites on the zirconia, and the As(III) uptake led to the release of HSO_4^- from the zirconia resulting in a decrease of pH. The adsorbed As(III) may form bidentate inner-sphere complexes on the surface of the sorbent.

Acknowledgements

The authors would like to express their appreciation to Agency for Science, Technology and Research of Singapore (Grant No. 0-921-010-059, and R-288-000-066-305) and Exploit Technologies Pte Ltd (R-398-000-078-592) for financial supports of this study. The PhD Scholarship to Ling Yu funded by Singapore Peking Oxford Research Enterprise (SPORE) is appreciated.

References

[1] P.L. Smedley, D.G. Kinniburgh, A review of the source, behavior and distribution of arsenic in natural waters, Appl. Geochem. 17 (2002) 517–568.
[2] A. Mudhoo, S.K. Sharma, V.K. Garg, C.H. Tseng, Arsenic: an overview of application, health, and environmental concerns and removal processes, Crit. Rev. Environ. Sci. Technol. 41 (2011) 435–519.
[3] Y.G. Zhu, G.X. Sun, M. Lei, M. Teng, Y.X. Liu, N.C. Chen, L.H. Wang, A.M. Carey, C. Deacon, A. Raab, A.A. Meharg, P.N. Williams, High percentage inorganic arsenic content of mining impacted and nonimpacted Chinese rice, Environ. Sci. Technol. 42 (2008) 5008–5013.
[4] X. Zhao, B.F. Zhang, H.J. Liu, J.H. Qu, Removal of arsenite by simultaneous electro-oxidation and electro-coagulation process, J. Hazard. Mater. 184 (2010) 472–476.
[5] Y.T. Wei, Y.M. Zheng, J.P. Chen, Uptake of methylated arsenic by a polymeric adsorbent: process performance and adsorption chemistry, Water Res. 45 (2011) 2290–2296.
[6] Y.M. Zheng, S.F. Lim, J.P. Chen, Preparation and characterization of zirconium-based magnetic sorbent for arsenate removal, J. Colloid Interface Sci. 338 (2009) 22–29.
[7] G.J. Liu, X.R. Zhang, J.W. Talley, C.R. Neal, H.Y. Wang, Effect of NOM on arsenic adsorption by TiO_2 in simulated As(III)-contaminated raw waters, Water Res. 42 (2008) 2309–2319.
[8] K. Grover, S. Komarneni, H. Katsuki, Uptake of arsenite by synthetic layered double hydroxides, Water Res. 43 (2009) 3884–3890.
[9] Z. Li, S. Deng, G. Yu, J. Huang, V.C. Lim, As(V) and As(III) removal from water by a Ce–Ti oxide adsorbent: behavior and mechanism, Chem. Eng. J. 161 (2010) 106–113.
[10] M.J. Kim, J. Nriagu, Oxidation of arsenite in groundwater using ozone and oxygen, Sci. Total Environ. 247 (2000) 71–79.

[11] Y. Lee, I.H. Um, J. Yoon, Arsenic(III) oxidation by iron(VI) (ferrate) and subsequent removal of arsenic(V) by iron(III) coagulation, Environ. Sci. Technol. 37 (2003) 5750–5756.
[12] D. Lakshmanan, D.A. Clifford, G. Samanta, Comparative study of arsenic removal by iron using electrocoagulation and chemical coagulation, Water Res. 44 (2010) 5641–5652.
[13] M. Sen, A. Manna, P. Pal, Removal of arsenic from contaminated groundwater by membrane-integrated hybrid treatment system, J. Membr. Sci. 354 (2010) 108–113.
[14] T.F. Lin, J.K. Wu, Adsorption of arsenite and arsenate within activated alumina grains: equilibrium and kinetics, Water Res. 35 (2001) 2049–2057.
[15] Y. Salameh, N. Al-Lagtah, M.N.M. Ahmad, S.J. Allen, G.M. Walker, Kinetic and thermodynamic investigations on arsenic adsorption onto dolomitic sorbents, Chem. Eng. J. 160 (2010) 440–446.
[16] S.J. Hug, O. Leupin, Iron-catalyzed oxidation of arsenic(III) by oxygen and by hydrogen peroxide: pH-dependent formation of oxidants in the fenton reaction, Environ. Sci. Technol. 37 (2003) 2734–2742.
[17] D. Lièvremont, M.A. N'negue, P. Behra, M.C. Lett, Biological oxidation of arsenite: batch reactor experiments in presence of kutnahorite and chabazite, Chemosphere 51 (2003) 419–428.
[18] F.S. Zhang, H. Itoh, Photocatalytic oxidation and removal of arsenite from water using slag–iron oxide–TiO_2 adsorbent, Chemosphere 65 (2006) 125–131.
[19] S. Sorlini, F. Gialdini, Conventional oxidation treatment for the removal of arsenic with chlorine dioxide, hypochlorite, potassium permanganate and monochloramine, Water Res. 44 (2010) 5653–5659.
[20] X. Zhao, B.F. Zhang, H.J. Liu, J.H. Qu, Simultaneous removal of arsenite and fluoride via an integrated electro-oxidation and electrocoagulation process, Chemosphere 83 (2011) 726–729.
[21] J. Zobrist, Mobilization of arsenite by dissimilatory reduction of adsorbed arsenate, Environ. Sci. Technol. 34 (2000) 4747–4753.
[22] M.E. Pena, G.P. Korfiatis, M. Patel, L. Lippincott, X.G. Meng, Adsorption of As(V) and As(III) by nanocrystalline titanium dioxide, Water Res. 39 (2005) 2327–2337.
[23] S.R. Kanel, B.M. Manning, L. Charlet, H. Choi, Removal of arsenic (III) from groundwater by nanoscale zero-valent iron, Environ. Sci. Technol. 39 (2005) 1291–1298.
[24] K. Gupta, U.C. Ghosh, Arsenic removal using hydrous nanostructure iron(III)–titanium(IV) binary mixed oxide from aqueous solution, J. Hazard. Mater. 161 (2009) 884–892.
[25] A. Sharma, N. Verma, A. Sharma, D. Deva, N. Sankararamakrishnan, Iron doped phenolic resin based activated carbon micro and nanoparticles by milling: synthesis, characterization and application in arsenic removal, Chem. Eng. Sci. 65 (2010) 3591–3601.
[26] K. Gupta, A. Maity, U.C. Ghosh, Manganese associated nanoparticles agglomerate of iron(III) oxide: synthesis, characterization and arsenic(III) sorption behavior with mechanism, J. Harzard. Mater. 184 (2010) 832–842.
[27] B. Prasad, C. Ghosh, A. Chakraborty, N. Bandyopadhyay, R.K. Ray, Adsorption fo arsenite (As^{3+}) on nano-sized Fe_2O_3 waste powder from the steel industry, Desalination 274 (2011) 105–112.
[28] N. Seko, F. Basuki, M. Tamada, F. Yoshii, Rapid removal of arsenic(V) by zirconium(IV) loaded phosphoric chelate adsorbent synthesized by radiation induced graft polymerization, React. Funct. Polym. 59 (2004) 235–241.
[29] A. Bortun, M. Bortun, J. Pardini, S.A. Khainakov, J.R. García, Effect of competitive ions on the arsenic removal by mesoporous hydrous zirconium oxide from drinking water, Mater. Res. Bull. 45 (2010) 1628–1634.
[30] Y.M. Zheng, S.W. Zou, K.G.N. Nanayakkara, T. Matsuura, J.P. Chen, Adsorptive removal of arsenic from aqueous solution by a PVDF/zirconia blend flat sheet membrane, J. Membr. Sci. 374 (2011) 1–11.
[31] Y. Ma, Y.M. Zheng, J.P. Chen, A zirconium based nanoparticle for significantly enhanced adsorption of arsenate: synthesis, characterization and performance, J. Colloid Interface Sci. 354 (2011) 785–792.
[32] S. Maity, S. Chakravarty, S. Bhattacharjee, B.C. Roy, A study on arsenic adsorption on polymetallic sea nodule in aqueous medium, Water Res. 39 (2005) 2579–2590.
[33] W.D. Schecher, MINEQL+: a Chemical Equilibrium Program for personal Computers, User Manual, Version 4.5, Environmental Research Software, Hallowell, ME, 2002.
[34] K.F. Hayes, C. Papelis, J.O. Leckie, Modeling ionic strength effects on anion adsorption at hydrous oxide/solution interfaces, J. Colloid Interface Sci. 125 (1988) 717–726.
[35] Y.S. Ho, G. McKay, Pseudo-second order model for sorption processes, Process Biochem. 34 (1999) 451–465.
[36] W.J. Weber, J.C. Morris, Kinetics of adsorption on carbon from solutions, J. Sanit. Eng. Div. ASCE 89 (1963) 31–60.
[37] V. Vadivelan, K.V. Kumar, Equilibrium, kinetics, mechanism, and process design for the sorption of methylene blue onto rice husk, J. Colloid Interface Sci. 286 (2005) 90–100.
[38] F.C. Wu, R.L. Tseng, R.S. Juang, Initial behavior of intraparticle diffusion model used in the description of adsorption kinetics, Chem. Eng. J. 153 (2009) 1–8.
[39] S.J. Zhang, X.Y. Li, J.P. Chen, Preparation and evaluation of a magnetite-doped activated carbon fiber for enhanced arsenic removal, Carbon 48 (2010) 60–67.
[40] G.M. Walker, L. Hansen, J.A. Hanna, S.J. Allen, Kinetics of a reactive dye adsorption onto dolomitic sorbents, Water Res. 37 (2003) 2081–2089.
[41] S.J. Allen, G. Mckay, J.F. Porter, Adsorption isotherm models for basic dye adsorption by peat in single and binary component systems, J. Colloid Interface Sci. 280 (2004) 322–333.
[42] L. Yang, S.N. Wu, J.P. Chen, Modification of activated carbon by polyaniline for enhanced adsorption of aqueous arsenate, Ind. Eng. Res. Chem. 46 (2007) 2133–2140.
[43] S. Depalma, S. Cowen, T. Hoang, H.A. Al-abadleh, Adsorption of thermodynamics of p-arsanilic acid on iron (oxyhydr) oxides: in-situ ATR-FTIR studies, Environ. Sci. Technol. 42 (2008) 1922–1927.
[44] E.A. Deliyanni, L. Nalbandian, K.A. Matis, Adsorption removal of arsenates by a nanocrystalline hybrid surfactant–akaganeite sorbent, J. Colloid Interface Sci. 302 (2006) 458–466.